Int. J. Nanosci. Nanotechnol., Vol. 17, No. 1, March 2021, pp. 41-53

Eco-Friendly Fabrication of Fe_3O_4/MWCNT/ZnO Nanocomposites from Natural Sand for Radar Absorbing Materials

Ahmad Taufiq[1,*], ST. Ulfawanti Intan Subadra[1], Nurul Hidayat[1], Sunaryono[1], Arif Hidayat[1], Erfan Handoko[2], Munasir[3], Mudrik Alaydrus[4] and Leamthong Chuenchom[5]

[1]Department of Physics, Faculty of Mathematics and Natural Sciences, Universitas Negeri Malang, Indonesia
[2]Department of Physics, Faculty of Mathematics and Natural Sciences, Universitas Negeri Jakarta, Indonesia
[3]Department of Physics, Faculty of Mathematics and Natural Sciences, Universitas Negeri Surabaya, Indonesia
[4]Department of Electrical Engineering, Universitas Mercu Buana, Indonesia
[5]Department of Chemistry, Prince of Songkla University, Thailand

(*) Corresponding Author: ahmad.taufiq.fmipa@um.ac.id
(Received: 03 July 2020 and Accepted: 03 December 2020)

Abstract

This paper reports on the fabrication of Fe_3O_4/MWCNT/ZnO nanocomposites (NCs) using natural iron sand as the primary precursor for radar absorbing materials. The addition of ZnO nanoparticles (NPs) was carried out to enhance the radar absorption performance of Fe_3O_4/MWCNT/ZnO NCs by improving their impedance. The X-ray diffraction patterns of Fe_3O_4/MWCNT/ZnO NCs demonstrated the inverse spinel cubic and hexagonal wurtzite structures for Fe_3O_4 NPs and ZnO NPs, respectively. The infrared spectra showed the presence of C=C, Fe-O, and Zn-O functional groups, which exhibited characteristics of MWCNT, Fe_3O_4, and ZnO, respectively. Such results were also confirmed by the results of energy dispersive X-ray investigation showing elements C, O, Fe, and Zn. The Fe_3O_4/MWCNT/ZnO NCs with superparamagnetic character decreased their saturation magnetization values due to the increasing ZnO NPs composition. Based on the optical data analysis, the bandgap energy of Fe_3O_4/MWCNT/ZnO NCs increased from 2.242 to 3.533 eV as the increasing ZnO NPs. Interestingly, the Fe_3O_4/MWCNT/ZnO NCs had a very high radar-absorbing performance ranging from 90%–99% with an optimum reflection loss of −34.2 dB at a frequency of 11.8 GHz. Thus, it implies that the Fe_3O_4/MWCNT/ZnO NCs provide a great opportunity as new material for developing radar-absorbing applications. Furthermore, the use of iron sand, which is economical and abundant in nature, has a very promising potential for producing large-scale antiradar materials.

Keywords: *Fe_3O_4/MWCNT/ZnO, Natural iron sand, Nanocomposite, Radar absorbing material, Reflection loss.*

1. INTRODUCTION

In the last decades, the need for radar absorbing materials (RAM) is ever-escalating in various applications, especially in military applications [1]. In general, the improvement of RAM-based technology in the military field is essential to a country's protection and defense [2], specifically for the development of weapons for the war [3], including for aircraft and battleships [4]. In terms of practical applications for the benefit of fighter aircraft, RAM works with the stealth system by reducing the radar cross-section, thereby plummeting the reflection of radar to improve the success of combat operations since the target is difficult to detect [5]. Therefore, experts in various fields, particularly in the nanoscience and nanotechnology realm, continue to develop a variety of fabrication methods to produce

new materials that have superior properties to RAM. To improve RAM performance, in general, it must be equipped with excellent characteristics, i.e., the excellent dielectric and magnetic properties [6], low density, and wide bandwidth [7]. Theoretically, these characteristics are of paramount importance since the radar has a magnetic and dielectric component in the form of directed perpendicular [8].

One of the magnetic materials that are currently being intensively developed by experts as RAM is Fe_3O_4. Some of the fundamental reasons underlying the development of Fe_3O_4 is because this material has an inverse spinel cubic structure with high magnetization [9], high permeability, low coercivity, strong mechanical properties [10], and high flexibility [11]. Unfortunately, research results show that Fe_3O_4 has limitations due to its relatively high density [9]. Furthermore, to achieve maximum performance of RAM by enhancing its absorption of radar, low-density materials are needed.

To enhance the radar absorption performance of RAM, researchers have previously shown that carbon nanotubes (CNT) have several properties that can mask the deficiency of Fe_3O_4, such as low density [6], qualified electrical properties [12], excellent mechanical properties [13], and a large surface area so that it can cover a wider uptake [14]. Thus, CNT provides a unique opportunity to be composited with Fe_3O_4 to improve its dielectric loss performance so that the RAM performance increases. Interestingly, multi-wall carbon nanotubes (MWCNT) as one type of CNT are also starting to be developed as a candidate for absorbing waves with a range between ultraviolet and visible light [15]. In addition to having the advantages of CNT properties such as density and excellent mechanical properties [16], MWCNT also has a high permittivity at a frequency of 8–18 GHz, resulting in broader bandwidth to increase antiradar capability [17]. However, previous research has shown that Fe_3O_4/MWCNT composite performance is not optimal for RAM applications due to its low reflection loss (*RL*) [18]. The low R_L of such composite is because of weak impedance matching between the surface of the material and the vacuum [8,9]. Therefore, it is essential to develop materials that can improve impedance matching. In this context, zinc oxide (ZnO) nanoparticles (NPs) provide an excellent opportunity to become composites in the Fe_3O_4/MWCNT/ZnO system. The importance of the ZnO NPs addition is in its semiconductor material [19], which has a specific surface area with a large pore volume [20], and high permeability and complex permittivity values [21]. Thus, the presence of ZnO NPs is believed to be able to improve the impedance matching performance of the composites [18].

Hitherto, research reports related to the development of Fe_3O_4/MWCNT/ZnO NCs for antiradar applications are rarely found. One report was found associated with the synthesis of Fe_3O_4/MWCNT/ZnO NCs using the in situ method and had an R_L in the range of –21.6 to –38.2 dB [18]. In another report, Fe_3O_4/MWCNT/ZnO NCs were also successfully synthesized by the thermolysis method and had a reflection value of –33.6 dB [22]. However, the primary precursors used in the synthesis of such NCs are still commercially priced. Thus, it requires high costs and is less suitable for large-scale production. Therefore, in this work, we developed the synthesis method of Fe_3O_4/MWCNT/ZnO NCs using the eco-friendly method by utilizing the abundant natural iron sand as the primary precursor. Furthermore, to investigate the performance of Fe_3O_4/MWCNT/ZnO NCs for antiradar applications, we investigated the effect of ZnO compositions on the antiradar performance. Moreover, for completing the study, we also investigated the structural, magnetic, and optical behavior of the Fe_3O_4/MWCNT/ZnO NCs.

2. MATERIALS AND METHODS

2.1. Synthesis of Fe_3O_4/MWCNT/ZnO NCs

The materials used in this study were iron sand, HCl (Merck, 12 M), NH_4OH (Merck, 14 M), MWCNT (Sigma Aldrich, ~ 50 nm in diameter, and ~ 1 μm in length), HNO_3 (Merck, 37%), $Zn(CH_3CO_2)_2{\cdot}2H_2O$ (Merck), NaOH (Merck, 3M), deionized water, ethanol, methanol, and distilled water. The iron sand contained a purity of 99.5% Fe_3O_4 powder after the separation process using a permanent magnet. The synthesis was started by the functionalization process of MWCNT using HNO_3 with the mass ratio of MWCNT and HNO_3 of 1:100. MWCNT was reacted with HNO_3 and sonicated for 2 h at a frequency of 40 kHz. The obtained product was then washed using distilled water and ethanol. Furthermore, the purification process of iron sands using a magnetic bar following our previous research procedure [23]. The 20 g of purified iron sand was reacted with HCl to obtain a solution containing $FeCl_3$ and $FeCl_2$. Next, 10 mL of the solution was reacted with 0.1 g of MWCNT through a sonication process for 10 min and continued with a titration process with 14 mL of NH_4OH. From such a reaction, the Fe_3O_4/MWCNT precipitate (dark black) was formed. The precipitate was washed repeatedly using distilled water and heated for 5 h at 100 ^oC to obtain the Fe_3O_4/MWCNT powders. Meanwhile, the ZnO NPs were synthesized using the sol-gel method. A total of 6.57 g of $Zn(CH_3CO_2)_2{\cdot}2H_2O$ was mixed with deionized water and stirred using a magnetic stirrer at a speed of 720 rpm followed by NaOH titration until a pH of 13 obtained. Afterward, the solution was precipitated and washed using methanol to achieve a neutral pH condition. Then, the solution was filtered and dried for 1 h at 100 ^oC to obtain the ZnO NPs. The Fe_3O_4/MWCNT NCs were mixed with distilled water using an ultrasonic bath for 30 min. Next, the ZnO NPs were mixed with Fe_3O_4/MWCNT/ZnO NCs in the solution using a magnetic stirrer for 30 min at room temperature. Furthermore, the solution was filtered and dried at 100 ^oC to produce the Fe_3O_4/MWCNT/ZnO NCs. The synthesis of Fe_3O_4/MWCNT/ZnO NCs was carried out with variations in the mass ratio of the Fe_3O_4/MWCNT NCs and ZnO NPs of 1:0; 1:0.5; 1:1, 1:2; 1:4, which were subsequently coded by FMZ 0, FMZ 1, FMZ 2, FMZ 3, and FMZ 4. Furthermore, the MWCNT/ZnO sample without Fe_3O_4 was coded by FMZ 5 with the mass ratio of the MWCNT and ZnO of 1:30 (0.1 g for MWCNT and 3 g for ZnO).

2.2. Characterizations

The crystal phase and structure of the Fe_3O_4/MWCNT/ZnO NCs were analyzed using an X-ray diffractometer (XRD). The XRD machine from X'Pert Pro, Pan Analytical, Netherlands, was maintained using Cu–Kα radiation with the wavelength of 1.5406 Å and 2θ with the values of $10°-80°$. The characterization of functional groups of the samples was done using Fourier-transform infrared spectros-copy. The morphology and elemental content were analyzed using scanning electron microscopy and energy-dispersive X-ray spectroscopy (SEM-EDAX), respectively. The SEM-EDAX machine (FEI Company, Inspect-S50) was employed with a magnification of 150,000×. The optical features of the samples were characterized using ultraviolet-visible spec-troscopy (UV-Vis) with the specification of UV-1700 PharmaSpec (Shimadzu). A vibrating sample magnetometer (VSM; VSMI.2H, Oxford Instrument) was employed to investigate the magnetic features of the samples. Furthermore, the potential of Fe_3O_4/MWCNT/ZnO NCs for antiradar applications was investigated using a vector network analyzer (VNA) measuring reflection and transmission signals in the frequency range of 7–13 GHz by calculating its reflection loss. In this experiment, the Fe_3O_4/MWCNT/ZnO NCs were mixed with epoxy resin with a mass ratio of 3:1. The samples were then

prepared with the dimension of the length of 22.8 mm and width of 10.1 mm.

3. RESULTS AND DISCUSSION

The diffraction patterns of the Fe_3O_4/MWCNT/ZnO NCs are shown in Figure 1. For the FMZ 0 sample, which represents the Fe_3O_4/MWCNT NCs, the qualitative data analysis demonstrating the diffraction peaks for the Fe_3O_4 were observed at 2θ of 30.3^o, 35.7^o, 47.4^o, 43.4^o, 53.8^o, 57.4^o, and 63.0^o. The result corresponds to the respective hkl planes of (220), (311), (400), (331), (442), (511), and (440). The highest diffraction peak observed in this work was in line with the results of previous work [24]. Furthermore, the quantitative analysis by a fitting approach using AMCSD No. 0007394 presented that the Fe_3O_4/MWCNT NCs constructed an inverse spinel cubic with the lattice parameters of approximately $a = b = c = 8.353$ Å and crystallite size of 6.13 nm. For the FMZ 0 sample, the diffraction peaks of MWCNT were not observed because its composition was too small compared to the diffraction peaks of Fe_3O_4. Also, the absence of MWCNT diffraction peaks was due to the high dispersion degree of MWCNT, indicating the Fe_3O_4 NPs that could be spread evenly on the surface of MWCNT [25].

The increasing ZnO NPs content in the Fe_3O_4/MWCNT/ZnO NCs can be observed from their diffraction peaks, as shown in Figure 1. Qualitatively, the increasing ZnO NPs is marked by the increasing peak intensity of ZnO NPs. In addition, the diffraction peaks of the ZnO NPs were detected at 2θ of 31.7^o, 34.5^o, 36.3^o, 47.6^o, 56.6^o, and 63.0^o. It represents the respective hkl planes of (010), (002), (011), (012), (110), and (013) originating from the ZnO NPs with hexagonal wurtzite structure [26]. The phase analysis for ZnO NPs was conducted using AMCSD No. 0005203. The lattice parameters of ZnO NPs were $a = b$ ranging from 3.247 to 3.253 Å and c ranging from 5.203 to 5.212 Å. For FMZ 0, the main diffraction peak of the Fe_3O_4 was detected at $2\theta = 35.7^o$. Meanwhile, for FMZ 1, the main diffraction peak tended to disappear due to the overlapping with the diffraction peak of ZnO [27]. Quantitatively, the increasing ZnO composition increased the crystallinity of Fe_3O_4/MWCNT/ZnO NCs, from 3.32% (without ZnO NPs) to 7.88%, 13.89%, 22.15%, 32.48%, and 42.52% for the respective FMZ 1, FMZ 2, FMZ 3, FMZ 4, and FMZ 5. Thus, the higher composition of ZnO NPs decreased the peak intensity of Fe_3O_4 NPs. The increasing ZnO composition increased the diffraction peak intensity of ZnO and generated a decrease in the diffraction peak intensity of Fe_3O_4. Interestingly, the diffraction peaks for FMZ 2-5 disappeared. Moreover, like FMZ 0, the diffraction peaks of MWCNT for FMZ 5 disappeared because the mass composition of MWCNT very low compared to those of ZnO.

SEM images of the Fe_3O_4/MWCNT NCs (FMZ 0) are shown in Figure 2. Based on the figure, the Fe_3O_4 NPs are attached to MWCNT in spherical aggregate form. Based on the electron microscopy images, it can be seen that the FMZ 0-5 samples had spherical particles representing the Fe_3O_4 bound to the surface of tube-like structures representing MWCNT. This phenomenon is originated from the agglomeration of Fe_3O_4 NPs spreading on the MWCNT's surface, which builds a pile of carbon in the form of bundles [24]. In addition, the Fe_3O_4 NPs bounds to the surface of MWCNT are also caused by interactions between particles provoked by the magnetic forces [28]. Theoretically, positive ions of Fe^{2+} and Fe^{3+} from the Fe_3O_4 are bound by negatively charged carboxyl groups on the surface of MWCNT that arise due to the functionalization process using nitric acid [29]. Therefore, it can be inferred that the treatment with acid successfully defects the MWCNT part and carboxyl groups form [30]. This treatment aimed to improve the ability of MWCNT to interact with other materials because there are carboxyl groups that bind to other materials [31]. Moreover,

the bright colour of the aggregated articles (not tube-like structures) is from the chemical elements with higher atomic numbers resulting in backscattered electrons (BSEs). Based on the chemical periodic table, it is known that the atomic number of Fe is 26 and Zn is 30. Therefore, it can be concluded that the bright colour represents ZnO while the dark colour represents Fe_3O_4.

Furthermore, the addition of ZnO composition caused the surface of the MWCNT to form a bundle covered with more nanoparticles. The results of previous research indicate that this phenomenon contributes to the evenly spread ZnO NPs on the surface of MWCNT [18]. This is supported by the results of the EDAX characterization shown in Table 1, where the carbon content, which is a characteristic of MWCNT, decreases as the composition of ZnO NPs increases. Logically, this also reduces the elemental content of Fe_3O_4 in the Fe_3O_4/MWCNT/ZnO NCs. Based on Table 1, it can be seen that FMZ 5 has the lowest C composition than other samples. For FMZ 5, the MWCNT as the main source of C was maintained with the lowest composition with the mass ratio of the MWCNT and ZnO of 1:30.

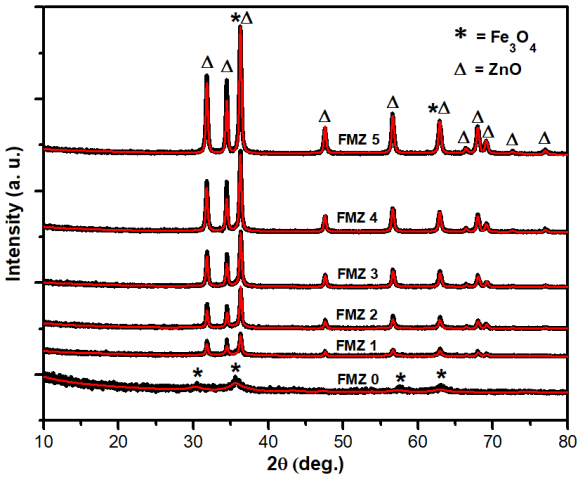

Figure 1. *Diffraction patterns of the Fe_3O_4/MWCNT/ZnO NCs.*

The infrared spectra of Fe_3O_4/MWCNT/ZnO NCs are shown in Figure 3. The presence of Fe_3O_4 was observed at wavenumbers of 586 cm^{-1} and 418 cm^{-1}, which respectively showed vibrations of Fe-O in tetrahedral and octahedral positions. Furthermore, the presence of such Fe-O vibrations also supported the results of X-ray diffraction data analysis showing that the Fe_3O_4 NPs form an inverse spinel cubic system. The emergence of Fe-O vibrations was also observed in the previous research at wavenumbers of 417 cm^{-1} [32] and 580–590 cm^{-1} [33].

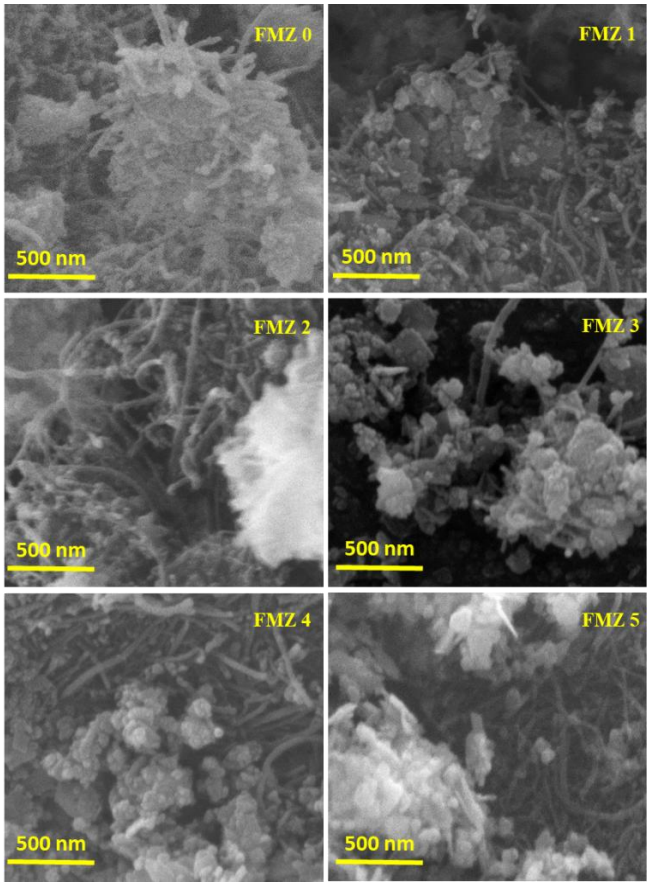

Figure 2. *SEM images of the Fe_3O_4/MWCNT/ZnO NCs.*

Table 1. *Elemental composition of the Fe_3O_4/MWCNT/ZnO NCs.*

Sample	Composition (Wt%)			
	C	O	Fe	Zn
FMZ 0	11.8	16.9	71.3	-
FMZ 1	24.7	11.7	36.7	26.9
FMZ 2	20.4	17.3	32.9	29.4
FMZ 3	15.2	11.9	19.5	53.4
FMZ 4	11.3	10.5	9.6	68.6
FMZ 5	3.6	13.5	-	82.9

All samples showed the absorption of the C=C functional group at 1650 cm^{-1}, where the functional group was a stretching vibration of carbon [30]. Thus, it proved the existence of MWCNT. This was also confirmed by several previous studies, where the vibration of the C=C functional group was observed at the wavenumbers of 1660 cm^{-1} and 1620–1680 cm^{-1} [34,35]. In addition, the stretching groups of C=O, C-H, and O-H were also detected as carboxyl groups due to the functionalization of MWCNT using acid [18]. Theoretically, the emergence of carboxyl groups on the surface of the MWCNT serves to improve the MWCNT to be able to attract other materials such as metal oxides, which in the context of this research are Fe_3O_4 NPs.

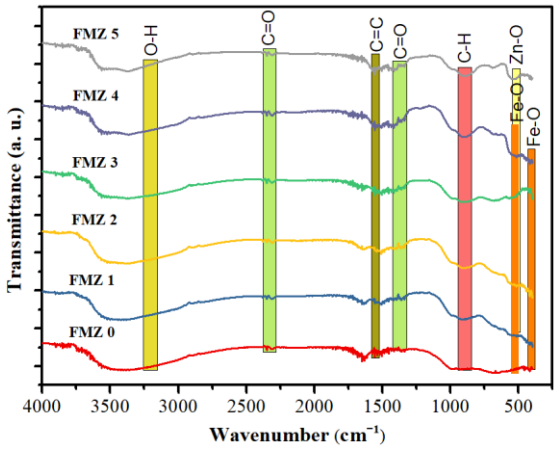

Figure 3. *FTIR spectra of the Fe_3O_4/MWCNT/ZnO NCs.*

The presence of ZnO NPs was detected at a wavenumber of 542 cm^{-1} that overlaps with tetrahedral Fe-O vibrations. In the area of the wavenumbers between 505 and 561 cm^{-1}, the absorption intensity was relatively high. It indicates that the Zn-O functional groups increased due to the addition of ZnO composition so that Zn-O absorption was also high. The emergence of Zn-O vibrations was confirmed by previous studies that succeeded in detecting Zn-O vibrations at the wavenumbers of 424–672 cm^{-1} [36]. In addition, the wavenumber range of 800–900 cm^{-1}, which was the C-H bonding area out of plane bending, was the increasingly broader absorption for the increasing ZnO composition.

An ultraviolet-visible spectrometer characterized the optical properties of Fe_3O_4/MWCNT/ZnO, as depicted in Figure 4. A peak absorbance of FMZ 0 was detected at a wavelength of 510.5 nm originating from Fe_3O_4 [37]. Interestingly, the addition of ZnO composition resulted in a shift in absorbance from 510.5 nm to the lower wavelength area between 341 and 342 nm. Physically, the combination of two or more materials tends to shift the bandgap energy value due to a shift in the absorption peak of the composites [38]. Based on the previous research, the absorbance of ZnO was detected at a wavelength of 340–370 nm [39], which had a lower value compared to Fe_3O_4.

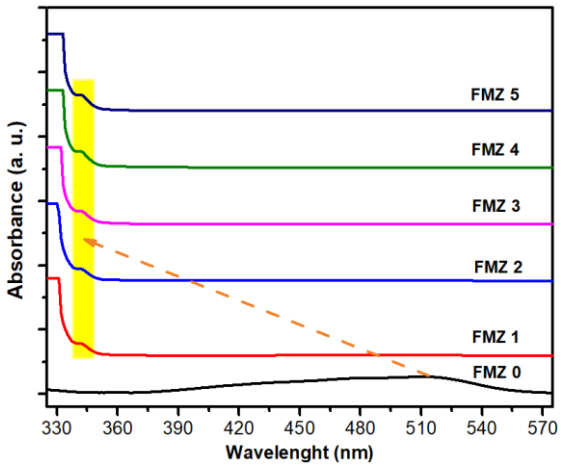

Figure 4. *Absorbance of the Fe_3O_4/MWCNT/ZnO NCs.*

Physically, the absorbance of Fe_3O_4/MWCNT/ZnO NCs is related to the energy needed by electrons to move from the valence band to the conduction band or better acknowledged as bandgap energy. In this study, the bandgap energy of the samples was calculated using the Kubelka Munk equation and analyzed using the Tauc Plot method. The results of the calculation are shown in Table 2. The bandgap energy value of the FMZ 0 is 2.242 eV. This value is close to the bandgap energy value of Fe_3O_4/CNT (2.3 eV), as shown by the previous study [40]. Furthermore, the bandgap energy values of

FMZ 1 to FMZ 5 range between 3.528 and 3.533 eV. The increasing bandgap energy value is due to a shift in absorbance peak from the rise in ZnO composition. In general, the bandgap energy value is close to the bandgap energy value from the previous result [41].

Table 2. *Bandgap energy of the Fe_3O_4/MWCNT/ZnO NCs.*

Sample	Wavelength (nm)	Bandgap Energy (eV)
FMZ 0	510.10	2.242
FMZ 1	341.29	3.530
FMZ 2	342.13	3.533
FMZ 3	341.24	3.532
FMZ 4	341.30	3.528
FMZ 5	342.19	3.499

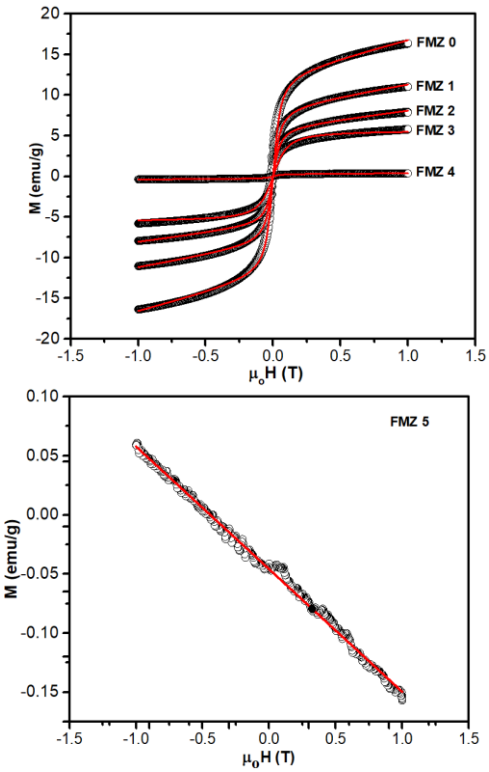

Figure 6. *Magnetization curves of the Fe_3O_4MWCNT/ZnO NCs.*

The magnetic properties of Fe_3O_4/MWCNT/ZnO NCs were characterized using a vibrating sample magnetometer at room temperature. Figure 6 shows the magnetization curves and their fitting using the Langevin Equation with the susceptibility shown in Equations 1–2:

$$M = Mr + Ms \times (\coth(C \times H) - \frac{1}{C \times H}) + \chi \times H \quad (1)$$

$$C = \frac{\mu}{k_B T} \quad (2)$$

where M is the magnetization, M_r is the remanent magnetization, M_s is the saturation magnetization, χ is the susceptibility, H is the magnetic field, T is the temperature, and k_B is the Boltzmann constant.

Table 3. *Magnetic properties of the Fe_3O_4MWCNT/ZnO NCs.*

Sample	M_s (emu/g)	M_r (emu/g)	H_c (T)
FMZ 0	12.64	0.09	0.01
FMZ 1	8.56	0.06	0.01
FMZ 2	6.09	0.02	0.01
FMZ 3	4.43	0.03	0.01
FMZ 4	0.29	0.00	0.01
FMZ 5	–	–	–

In this study, the FMZ 0 with a particle size of 6.13 nm has a saturation magnetization value of 12.64 emu/g. This value is higher than those of the Fe_3O_4/MWCNT (1.50 emu/g) with a particle size of 3 nm [42]. Consequently, the *M*s value of a material is influenced by particle size, where the larger particle size increases the magnetization value [43]. Besides *M*s, other parameters such as remanent magnetization (*M*r) and coercivity field (*H*c) were also analyzed and its results are shown in Table 3. The *M*r and *H*c values for the FMZ 0, FMZ 1, FMZ 2, FMZ 3, and FMZ 4 were very small so that they can be ignored. Therefore, the Fe_3O_4/MWCNT/ZnO NCs prepared in this experiment presented superparamagnetic properties [43]. Furthermore, the addition of ZnO composition decreased the *Ms* value of Fe_3O_4/MWCNT/ZnO NCs because of the decreasing Fe_3O_4 fraction. The FMZ 5 (MWCNT/ZnO) shown diamagnetic characteristics. Once it is given a positive external field, the magnetization is negative and vice versa. In other words, the material opposes a given external magnetic field.

Thus, it can be concluded that the FMZ 5 is a diamagnetic material [44].

Theoretically, excellent RAM should have characteristics of excellent electrical permittivity and magnetic permeability. The electrical permittivity refers to the complex permittivity (ε_r), where $\varepsilon_r = \varepsilon' - j\varepsilon''$ and the magnetic permeability refers to the complex permeability (μ_r), where $\mu_r = \mu' - j\mu''$ [45]. The complex relative permeability and permittivity of the Fe_3O_4/MWCNT/ZnO NCs were investigated in the frequency range of 7–13 GHz, as presented in Figure 8. In the figure, we can observe some important parameters, i.e., μ' that symbolizes the magnetic storage energy, and μ'' that symbolizes the magnetic energy dissipation. Meanwhile, the real (ε') and imaginary (ε'') parts correspond to the dielectric storage energy and dielectric energy dissipation of the electromagnetic energy [18].

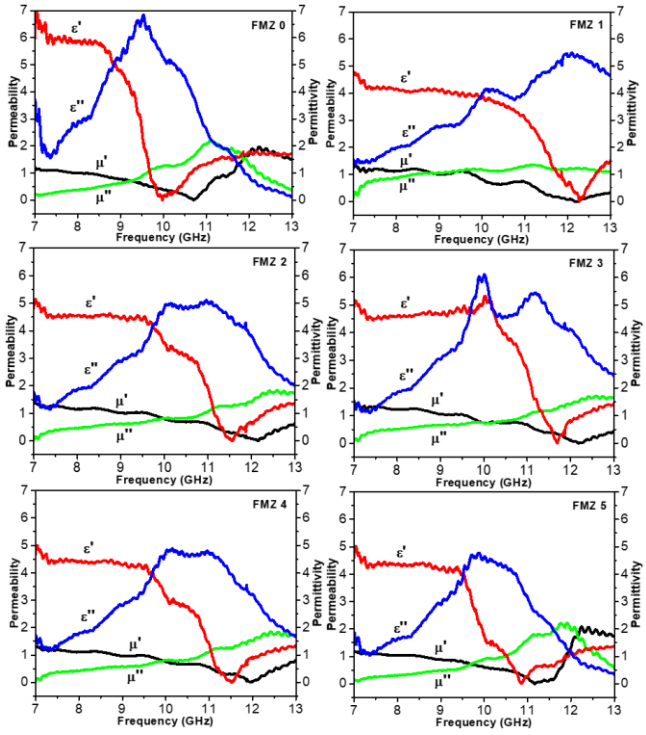

Figure 8. *Permeability and permittivity of the Fe_3O_4/MWCNT/ZnO NCs.*

The real μ' part of the samples had similar decreasing μ' values that increased at a particular frequency. According to the previous research, the μ' value of Fe_3O_4 is 1.17 [18]. On the other hand, in this study, the μ' value of Fe_3O_4/MWCNT NCs was 1.18 and decreased to zero at 10.7 GHz and increased afterward. Besides, the addition of ZnO increased the μ' value from 1.2 to 1.5. The increasing μ' value was closely related to the increasing dispersion of Fe_3O_4 after the additional MWCNT and ZnO. The imaginary curve of μ'' part tended to be similar to ε'' part.

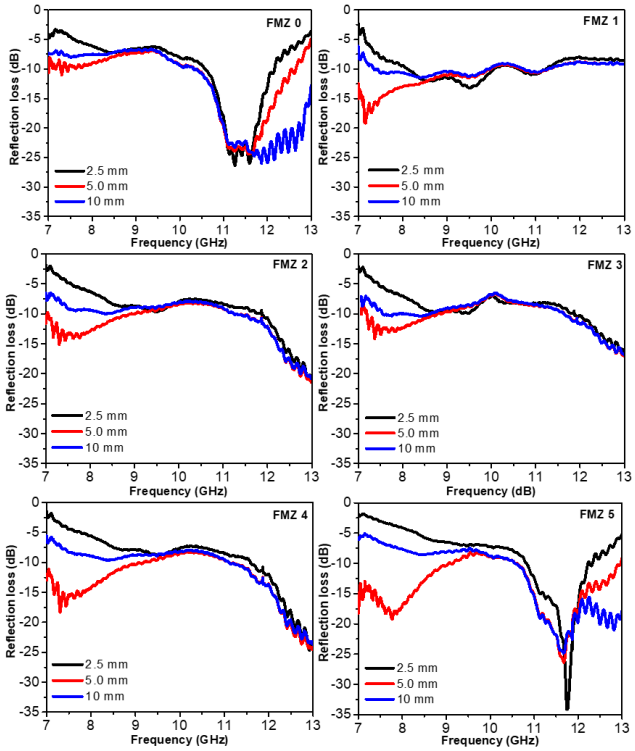

Figure 9. *Reflection loss of the Fe_3O_4/MWCNT/ZnO NCs with thickness variation.*

Furthermore, the ε' value of Fe_3O_4/MWCNT/ZnO NCs decreased along with increasing frequency. For the FMZ 0, the ε' decreased from 7 to 0 in the frequency range of 7–10 GHz accompanied by small fluctuations. For the FMZ 5, the ε' value also decreased from 5 to 0 in the frequency range of 7–11 GHz. Moreover, the addition of ZnO on the NCs produced a lower ε' value than those of the FMZ 0. However, there was a high resonance peak between the frequency of 11.5 and 12 GHz for all samples due to the addition of ZnO NPs. Principally, this phenomenon occurs because of the particle aggregation that happened on the nanocomposite over the

increasing composition of ZnO NPs [6], as presented in Figure 2. Every ε'' had the same trend that shows a deterioration in the frequency range of 7–8 GHz, then increased along with several fluctuations and decreased again. This indicates multiple resonances related to electronic spin, high conductivity, and polarization charge. The relatively high ε' and ε'' values indicate the high storage and loss ability of the microwave energy. This shows that the polar polarization, interfacial polarization, and energy storage of electromagnetic waves possessed by nanocomposites are high.

Table 4. *Reflection loss values of the Fe_3O_4MWCNT/ZnO NCs with thickness variation.*

Sample	2.5 mm		5.0 mm		10.0 mm	
	RL (dB)	Freq (GHz)	*RL* (dB)	Freq (GHz)	*RL* (dB)	Freq (GHz)
Fe_3O_4	-3.3 [22]	-	-	-	-	-
MW CNT	-3.0 [22]	-	-	-	-	-
ZnO	-1.1 [22]	-	-	-	-	-
FMZ 0	-26.4	11.3	-24.0	11.3	-23.3	11.3
FMZ 1	-13.2	9.5	-11.5	9.5	-11.3	9.5
FMZ 2	-9.7	9.0	-9.5	9.0	-9.0	9.0
FMZ 3	-10.0	9.5	-8.8	9.6	-8.6	9.5
FMZ 4	-8.8	9.5	-9.6	9.4	-9.7	9.5
FMZ 5	-34.2	11.8	-26.1	11.7	-24.9	11.7
ZnO@ MWCNT	-20.7 [48]	-	-	-	-	-

The ability of RAM to absorb radar is strongly related to reflection loss (*RL*). The *RL* values of the Fe_3O_4/MWCNT/ZnO NCs were calculated using Equations 3–4.

$$RL = 20\log\left|\frac{Z_{in} - Z_0}{Z_{in} + Z_0}\right| \quad (3)$$

$$Z_{in} = Z_0\sqrt{\mu_r\varepsilon_r}\tanh\left[j\frac{2\pi fd}{c}\sqrt{\mu_r\varepsilon_r}\right] \quad (4)$$

Where *RL* is the reflection loss (dB), Z_{in} is the input impedance, Z_o is the vacuum impedance value, μ_r and ε_r are the complex permeability and permittivity of the material, *and* c is the velocity of electromagnetic waves in a vacuum, f is the frequency of incident waves, and d is the thickness of the material [46].

Figure 9. shows the reflection loss of the Fe_3O_4/MWCNT/ZnO NCs. In principle, reflection loss is the ability of a material to absorb radar waves. Theoretically, the more negative *RL* value indicates lesser incoming waves fired to the materials [43]. Thus, the Fe_3O_4/MWCNT/ZnO NCs have high absorption and can be presented as excellent RAM. In this study, the R_L values of the Fe_3O_4/MWCNT/ZnO NCs were evaluated with thickness variations of 2.5, 5.0, and 10.0 mm, as presented in Table 4.

In this work, FMZ 0 and FMZ 5 become the best samples for antiradar application based on the reflection loss value. The *RL* values of FMZ 0 and FMZ 5 are relatively higher than other samples, originated from high magnetic and dielectric composition resulting in highly complex permeability and permittivity values [18]. Moreover, the addition of MWCNT also contributes a great deal to the *RL* values for FMZ 0 and FMZ 5, where the amount of surface suspension from MWCNT allows polarization and increases radar absorption [47]. However, based on the absorption frequency range, FMZ 1-4 become the best samples for antiradar application because they can absorb radar not only at high frequencies but also can absorb radar at low frequencies. Therefore, it is important to carry out further research by optimizing synthesis parameters, composition, and other aspects to obtain new materials with high reflection loss, not only at high frequencies.

Based on the results of previous research, Fe_3O_4 NPs with a thickness of 2.5 mm applied as RAM produced an *RL* value of –7.3 dB [48]. In this study, the Fe_3O_4/MWCNT NCs with different thicknesses had higher *RL* values compared to pure Fe_3O_4, ranging from –23.3 to –26.4 dB. Therefore, the results of this study were higher than previous studies that produced an *RL* value of –20.1 dB [49]. The increasing *RL* value was caused by the

presence of a dielectric component that absorbs the dielectric portion of the radar. In addition, the increasing *RL* value was also caused by the presence of electrostatic forces between the O-H groups on the MWCNT surface due to treatment with acidic solutions along with positive ions from Fe_3O_4. The forces caused Fe_3O_4 NPs to connect with MWCNT, facilitating electrons to jump and move as well as increasing the absorption of radar waves. Furthermore, the combination of ZnO and MWCNT in this study also showed high *RL* values from –24.9 to –34.2 dB. These results are more significant compared to previous studies that have succeeded in preparing ZnO/MWCNT as RAM with an *RL* value of –20.7 dB [48]. Meanwhile, the *RL* of the MWCNT and ZnO were –3.0 dB and –1.04 dB, respectively [22]. In this regard, the ZnO NPs deposited on the MWCNT surface decreased the conductivity of the MWCNT and increased the interfaces between the two materials, which changed the complex permittivity of the nanocomposite so that it got a matching impedance [18].

Table 4 represents the *RL* values for all samples with thickness variations. The results of this study indicated that the *RL* value of each sample tended to decline as the sample thickness increased. This is in accordance with the theory stating that the relationship between thickness and frequency match, where the thickness increases, the frequency match between the sample and the incident wave decrease [50]. The low-frequency match decreased the impedance match, creating an increase in radar reflection on the sample surface [18], thereby reducing the *RL* value at the same frequency. The *RL* value deterioration accompanied by the increasing thickness is explained by the quarter-wave principle. This principle explains that the electromagnetic wave partially subjected to the sample will be reflected from the air to the metal interface, and some of them will be reflected from the absorbant to the metal interface. Those two reflections will deprive one another once they fulfill quarter-wave thickness criteria. The criteria state that frequency matching is inversely proportional to the thickness [51]. Therefore, increasing the thickness provokes the disappearance of electromagnetic waves and the appearance of more reflected waves that increase the *RL*. In this work, the *RL* value of the Fe_3O_4/MWCNT/ZnO NCs ranged from –8.7 to –34.2 dB. Based on the results of previous studies, the *RL* values lower than –10 dB and –20 dB have the respective absorption rates of 90% and 99% [48]. Based on the calculation of R_L values, the Fe_3O_4/MWCNT/ZnO NCs obtained in this study have a very high absorption rate, ranging from 90% to 99%. Thus, the Fe_3O_4/MWCNT/ZnO NCs fabricated in this study provides an excellent opportunity to be applied as RAM, specifically to enhance a country's defense and capability in the military field.

4. CONCLUSION

The Fe_3O_4/MWCNT/ZnO NCs were successfully synthesized through precipitation methods with variations in the composition of ZnO NPs. The existence of the Fe_3O_4 and ZnO NPs was confirmed by the crystalline phases with inverse cubic spinel and hexagonal wurtzite structures, respectively. The morphology of the Fe_3O_4/MWCNT NCs tended to agglomerate as ZnO composition increases. The bandgap energy of the Fe_3O_4/MWCNT NCs ranged from 2.242 to 3.533 eV. The increasing ZnO NPs decreased the *RL* values of the Fe_3O_4/MWCNT NCs, which were caused by agglomeration. Interestingly, the produced Fe_3O_4/MWCNT/ZnO NCs were able to absorb electromagnetic waves in the range of 90%–99% with the *RL* value range from –8.7 to –34.2 dB.

ACKNOWLEDGEMENT

This work was financially supported by Universitas Negeri Malang and DRPM-DIKTI, the Republic of Indonesia, for AT.

REFERENCES

1. Qu, S., Wu, G., Fang, J., Zang, D., Xing, H., Wang, L., Wu, H., "*Dielectric and Magnetic Loss Behavior of Nanooxides in Spectroscopic Methods for Nanomaterials Characterization*", Elsevier, Belanda (2017).
2. Li, W., Lin, L., Li, C., Wang, Y., Zhang, J., "Radar Absorbing Combinatorial Metamaterial based on Silicon Carbide/Carbon Foam Material Embedded with Split Square Ring Metal", *Results in Physics*, 12 (2019) 278–86.
3. Li, W., Li, C., Lin, L., Wang, Y., Zhang, J., "All-Dielectric Radar Absorbing Array Metamaterial based on Silicon Carbide/Carbon Foam Material", *Journal of Alloys and Compounds*, 781 (2019) 883–91.
4. Wang, C., Chen, M., Lei, H., Yao, K., Li, H., Wen, W., Fang, D., "Radar Stealth and Mechanical Properties of a Broadband Radar Absorbing Structure", *Composites Part B: Engineering*, 123 (2017) 19–27.
5. Li, W., Zhang, Y., Wu, T., Cao, J., Chen, Z., Guan, J., "Broadband Radar Cross Section Reduction by in-Plane Integration of Scattering Metasurfaces and Magnetic Absorbing Materials", *Results in Physics*, 12 (2019) 1964–70.
6. Xia, R., Yin, Y., Zeng, M., Dong, H., Yang, H., Zeng, X., Tang, W., Yu, R., "High-Frequency Absorption of the Hybrid Composites with Spindle-like Fe_3O_4 Nanoparticles and Multiwalled Carbon Nanotubes", *Nano*, 11 (2016) 1650097.
7. Panwar, R., Puthucheri, S., Agarwala, V., Singh, D., "Effect of Particle Size on Radar Wave Absorption of Fractal Frequency Selective Surface Loaded Multilayered Structures", *IEEE*, (2014) 186–9.
8. Bhattacharya, P., Sahoo, S., Das, C. K., "Microwave Absorption Behaviour of MWCNT Based Nanocomposites in X-band Region", *Express Polymer Letters*, 7 (2013) 212–23.
9. Mingdong, C., Huangzhong, Y., Xiaohua, J., Yigang, L., "Optimization on Microwave Absorbing Properties of Carbon Nanotubes and Magnetic Oxide Composite Materials", *Applied Surface Science*, 434 (2018) 1321–1326.
10. Wei, S., Yan, R., Shi, B., Chen, X., "Characterization of Flexible Radar-Absorbing Materials based on Ferromagnetic Nickel Micron-Fibers", *Journal of Industrial Textiles*, 49 (2018) 58–70.
11. Yalçın, O., Bayrakdar, H., Özüm, S., "Spin-flop Transition, Magnetic and Microwave Absorption Properties of α-Fe_2O_4 Spinel Type Ferrite Nanoparticles", *Journal of Magnetism and Magnetic Materials*, 343 (2013) 157–62.
12. Al-Ghamdi, A. A., Al-Hartomy, O. A., Al-Solamy, F. R., Dishovsky, N., Nickolov, R., Atanasov, N., Ruskova, K., "Effect of Activated Carbon/In Situ Synthesized Magnetite Hybrid Fillers on the Microwave Properties of Natural Rubber Composites", *Advanced Materials Proceedings*, 2 (2017) 621–628.
13. Ye, W., Sun, Q., Zhang, G., "Effect of Heat Treatment Conditions on Properties of Carbon-Fiber based Electromagnetic Wave Absorbing Composites", *Ceramics International*, 45 (2019) 5093–5099.
14. Son, S. Y., Lee, D. H., Kim, S. D., Sung, S. W., Park, Y. S., Han, J. H., "Synthesis of Multi-Walled Carbon Nanotube in a Gas-Solid Fluidized Bed", *Korean Journal of Chemical Engineering*, 23 (2006) 838–841.
15. Kordhaghi, F., Sadrnezhaad, S. K., Doulabi, M., "Synthesis and Characterization of Anatase-coated Multiwall Carbon Nanotube for Improvement of Photocatalytic Activity", *International Journal of Engineering*, 30 (2017) 543–550.
16. Mahdavi, M., Khayati, G. R., "Artificial Neural Network Based Prediction Hardness of Al2024-Multiwall Carbon Nanotube Composite Prepared by Mechanical Alloying", *International Journal of Engineering*, 29 (2016) 1726–1733.
17. Das, C. K., Bhattacharya, P., Kalra, S. S., "Graphene and MWCNT: Potential Candidate for Microwave Absorbing Materials. Journal of Materials Science Research", *Journal of Materials Science Research*, 1 (2012) 126.
18. Wang, L., Xing, H., Liu, Z., Shen, Z., Sun, X., Xu, G., "Synthesis and Excellent Microwave Absorption Properties of ZnO/Fe_3O_4 /MWCNTs Composites", *Nano*, 11 (2016) 1650139.
19. Vafaee, M., Ghamsari, M., S., "Preparation and Characterization of ZnO Nanoparticles by a Novel Sol–gel Route", *Materials Letters*, 61 (2007) 3265–3268.
20. Ahamed, A. J., Kumar, P. V., "Synthesis and Characterization of ZnO Nanoparticles by Co-precipitation Method at Room Temperature", *Journal of Chemical and Pharmaceutical Research*, 8 (2016) 624–628.
21. Liu, X. G., Geng, D. Y., Meng, H., Shang, P. J., Zhang, Z. D., "Microwave-absorption Properties of ZnO-Coated Iron Nanocapsules", *Applied Physics Letters*, 92 (2008) 173117.
22. Wang, Z., Wu, L., Zhou, J., Jiang, Z., Shen, B., "Chemoselectivity-induced Multiple Interfaces in MWCNT/Fe_3O_4@ZnO Heterotrimers for whole X-band Microwave Absorption", *Nanoscale*, 6 (2014) 12298–12302.
23. Taufiq, A., Sunaryono, Hidayat, N., Hidayat, A., Putra, E. G. R., Okazawa, A. A.,Watanabe, I., Kojima, N., Pratapa, S., Darminto., "Studies on Nanostructure and Magnetic Behaviors of Mn-Doped Black Iron Oxide Magnetic Fluids Synthesized from Iron Sand", *Nano*, 12 (2017) 1750110.
24. Rahmawati, R., Melati, A., Taufiq, A., Diantoro, M., Yuliarto, B., Suyatman, S., Nugraha, N., Kurniadi, D., "Preparation of MWCNT-Fe_3O_4 Nanocomposites from Iron Sand using Sonochemical Route", *IOP Conference Series: Materials Science and Engineering*, 202 (2017) 012013.
25. Sobahi, T. R. A., Abdelaal, M. Y., Mohamed, R. M., Mokhtar, M., "Photocatalytic Degradation of Methylene Blue Dye in Water Using Pt/ZnO-MWCNT Under Visible Light", *Nanoscience and Nanotechnology Letters*, 9 (2017) 144–150.

26. Anaraki, F. A., Keyhani, M., "The Effect of Different Dopants (Cr, Mn,on (Cu and Ni ,Co ,Fe Photocatalytic Properties of ZnO Nanostructures", *International Journal of Nanoscience and Nanotechnology*, 16 (2020) 59–65.
27. Taufiq, A., Ulya, H. N., Yogihati, C. I., Sunaryono, Hidayat N., Mufti N., Soda, S., Ishida, T., "Effects of ZnO Nanoparticles on the Antifungal Performance of Fe_3O_4/ZnO Nanocomposites Prepared from Natural Sand", *Adv. Nat. Sci.: Nanosci Nanotechnol*, 11 (2020) 045004.
28. Rahmawati, R., Taufiq, A., Sunaryono, Yuliarto, B., Suyatman, Nugraha, Noviandri, I., Setyorini, D. A., Kurniadi, D., "The synthesis of Fe_3O_4/MWCNT Nanocomposites from Local Iron Sands for Electrochemical Sensors", *AIP Conference Proceedings*, 1958 (2018) 020016.
29. Fisli, A., Ariyani, A., Wardiyati, S., Yusuf, S., "Magnetic Adsorbent of Active Carbon-Fe_3O_4 Nanocomposite for Thorium Adsorption", *Indonesian Journal of Materials Science*, 13 (2012) 130490.
30. Zhao, Z., Yang, Z., Hu, Y., Li, J., Fan, X., "Multiple Functionalization of Multi-Walled Carbon Nanotubes with Carboxyl and Amino Groups", *Applied Surface Science*, 276 (2013) 476–481.
31. Aroon, M. A., Beheshti, H., Barzin, J., Shariaty-Niassar, M., "Purified and Functionalized MWCNTs: Application in CO_2/CH_4 Separation Using Mixed Matrix Membranes", *International journal of nanoscience and nanotechnology*, 14 (2018) 251–266.
32. Wang, B., Wang, B., Wei, P., Wang, X., Lou, W., "Controlled Synthesis and Size-dependent Thermal Conductivity of Fe_3O_4 Magnetic Nanofluids", *Dalton Transactions*, 41 (2012) 896–899.
33. Yusoff, A. H. M., Salimi, M. N., Jamlos, M. F., "Synthesis and Characterization of Biocompatible Fe_3O_4 Nanoparticles at Different pH", *AIP Conference Proceedings*, 1835 (2017) 020010.
34. Socrates, G., *"Infrared and Raman characteristic group frequencies: tables and charts"*, John Wiley & Sons, (2004).
35. Munasir, N., Kusumawati, R., P., Kusumawati, D. H., Supardi, Z. A. I., Taufiq, A., Darminto, "Characterization of Fe_3O_4/rGO Composites from Natural Sources: Application for Dyes Color Degradation in Aqueous Solution", *International Journal of Engineering*, 33 (2020) 18–27.
36. Sharma, D., Jha, R., "Transition metal (Co, Mn) Co-doped ZnO Nanoparticles: Effect on Structural and Optical Properties", *Journal of Alloys and Compounds*, 698 (2017) 532–538.
37. Feng, X., Guo, H., Patel, K., Zhou, H., Lou, X., "High Performance, Recoverable Fe_3O_4/ZnO Nanoparticles for Enhanced Photocatalytic Degradation of Phenol", *Chemical Engineering Journal*, 244 (2014) 327–334.
38. Fayemi, O. E., Adekunle, A. S., "Metal Oxide Nanoparticles/Multi-walled Carbon Nanotube Nanocomposite Modified Electrode for the Detection of Dopamine: Comparative Electrochemical Study", *Journal of Biosensors & Bioelectronics*, 6 (2015) 190.
39. Aquisman, A. E., Wee, B. S., Chin, S. F., Kwabena, D. E., Michael, K. O., Bakeh, T., Semawi, S., and Sylverster, D. P., "Synthesis, Characterization, andAntibacterial Activity of ZnO Nanoparticles from Organic Extract of Cola Nitida and ColaAcuminata Leaf", *International Journal of Nanoscience and Nanotechnology*, 16 (2020) 73–89.
40. Rahman, M. M., Hussain, M. M., Asiri, A. M., "Fabrication of 3-methoxyphenol Sensor based on Fe_3O_4 Decorated Carbon Nanotube Nanocomposites for Environmental Safety: Real Sample Analyses", *Plos One*, 12 (2017) e0177817.
41. Mazhdi, M., Hossein, K. P., "Structural Characterization of ZnO and ZnO: Mn Nanoparticles Prepared by Reverse Micelle Method", *International Journal of Nano Dimension*, 2 (2012) 233-240.
42. Ramezan, Z. M. H., Seifi, M., Hekmatara, H., Askari, M., B., "Preparation and study of the electrical, magnetic and thermal properties of Fe_3O_4 coated carbon nanotubes", *Chinese Journal of Physics*, 55 (2017) 1319–1328.
43. Taufiq, A., Bahtiar, S., Sunaryono, Hidayat, N., Hidayat, A., Mufti, N., Diantoro, M., Fuad, A., Rahmawati, R., Adi, W. A., Pratapa, S., "Preparation of Superparamagnetic $Zn_{0.5}Mn_{0.5}Fe_2O_4$ Particle by Coprecipitation-Sonochemical Method for Radar Absorbing Material", *IOP Conference Series: Materials Science and Engineering*, 202 (2017) 012024.
44. Cullity, B., D., Graham, C., D., *"Introduction to Magnetic Materials"*, John Wiley & Sons, USA, (2008).
45. Liu, C., Xu, Q., Tang, Y., Wang, Z., Ma, R., Ma, N., Du, P., "Zr^{4+} Doping-Controlled Permittivity and Permeability of $BaFe_{12-x}Zr_xO_{19}$ and The Extraordinary EM Absorption Power in The Millimeter Wavelength Frequency Range", *Journal of Materials Chemistry C. Royal Society of Chemistry*, 4 (2016) 9532–9543.
46. Molaei, M. J., Rahimipour, M. R., "Microwave Reflection Loss of Magnetic/Dielectric Nanocomposites of $BaFe_{12}O_{19}$/TiO_2", *Materials Chemistry and Physics*, 167 (2015) 145–151.
47. Tang, H., Jian, X., Wu, B., Liu, S., Jiang, Z., Chen, X., He, W. W., Tian, W., Wei, Y., Gao, Y., Chen, T., Li, G., "Fe_3C/Helical Carbon Nanotube Hybrid: Facile Synthesis and Spin-Induced Enhancement in Microwave-Absorbing Properties", *Composites Part B: Engineering*, 107 (2016) 51–58.
48. Sun, D., Zou, Q., Wang, Y., Wang, Y., Jiang, W., Li, F., "Controllable Synthesis of Porous Fe_3O_4@ZnO Sphere Decorated Graphene for Extraordinary Electromagnetic Wave Absorption", *Nanoscale*, 6 (2014) 6557–6562.
49. Lu, M. M., Cao, W., Q., Shi, H. L., Fang, X. Y., Yang, J., Hou, Z. L., Wang, W. Z., Yuan, J., Cao, M. S., "Multi-Wall Carbon Nanotubes Decorated with ZnO Nanocrystals: Mild Solution-Process Synthesis and

Highly Efficient Microwave Absorption Properties at Elevated Temperature", *Journal of Materials Chemistry A : Royal Society of Chemistry*, 2 (2014) 10540–10547.
50. Idris, F. M., Hashim, M., Abbas, Z., Ismail, I., Nazlan, R., Ibrahim, I. R., "Recent Developments of Smart Electromagnetic Absorbers based Polymer-Composites at Gigahertz Frequencies", *Journal of Magnetism and Magnetic Materials*, 405 (2016) 197–208.
51. Abbas, S. M., Dixit, A. K., Chatterjee, R., Goel, T. C., "Complex permittivity, Complex Permeability and Microwave Absorption Properties of Ferrite–Polymer Composites", *Journal of Magnetism and Magnetic Materials*, 309 (2007) 20–24.